

## VHE Gamma-ray Observation of Crab Nebula with HAGAR Telescope Array

B.B. Singh\* · R.J. Britto · V.R. Chitnis · A. Shukla · L. Saha · A. Sinha · B.S. Acharya · P.R. Vishwanath · G.C. Anupama · P. Bhattacharjee · K.S. Gothe · B.K. Nagesh · T.P. Prabhu · S.K Rao · R. Srinivasan · S.S. Upadhya

Received: date / Accepted: date

**Abstract** HAGAR is a system of seven Non-imaging Atmospheric Cherenkov Telescopes located at Hanle in the Ladakh region of the Indian Himalayas at an altitude of 4270 meters *amsl*. Since 2008, we have observed the Crab Nebula to assess the performance of the HAGAR telescopes. We describe the analysis technique for the estimation of  $\gamma$ -ray signal amidst cosmic ray background. The consolidated results spanning nine years of the Crab nebula observations show long term performance of the HAGAR telescopes. Based on about 219 hours of data, we report the detection of  $\gamma$ -rays from the Crab Nebula at a significance level of about  $20\sigma$ , corresponding to a time averaged flux of  $(1.64 \pm 0.09) \times 10^{-10}$  photons  $\text{cm}^{-2} \text{sec}^{-1}$  above 230 GeV. Also, we perform a

\* Corresponding author E-mail: bbsingh@tifr.res.in

B.B. Singh · R.J. Britto · V.R. Chitnis · A. Sinha · B.S. Acharya · K.S. Gothe · B.K. Nagesh · S.K Rao · S.S. Upadhya  
Tata Institute of Fundamental Research, Homi Bhabha Road, Colaba, Mumbai 400005, India

A. Shukla · P.R. Vishwanath · G.C. Anupama · T.P. Prabhu · R. Srinivasan  
Indian Institute of Astrophysics, II Block, Koramangala, Bangalore 560034, India

L. Saha · P. Bhattacharjee  
Saha Institute of Nuclear Physics, 1/AF, Bidhannagar, Kolkata 700064, India

R.J. Britto  
Department of Physics, University of the Free State, PO Box 339, Bloemfontein 9300, South Africa

A. Shukla  
Institute for Theoretical Physics and Astrophysics, Universität Würzburg, 97074 Würzburg, Germany

L. Saha  
Universidad de Complutense, E-28040 Madrid, Spain

A. Sinha  
Astroparticule et Cosmologie/CNRS/ Universit Paris Diderot, Paris-75013

detailed study of possible systematic effects in our analysis method on data taken with the HAGAR telescopes.

**Keywords** Crab Nebula, Cherenkov Telescopes, VHE  $\gamma$ -rays

## 1 Introduction

Crab Nebula is the first source detected in very high energy (VHE)  $\gamma$ -rays [Weekes et al 1989] and extensively studied object by ground based atmospheric Cherenkov detectors. After the first light from the supernova (SN 1054) which was recorded in 1054 AD, it is one of the best studied non-thermal celestial objects in almost all energy bands of the electromagnetic spectrum. The Crab Nebula lies  $\approx 2$  kpc [Trimble 1968] from the Earth at a right ascension (RA) of  $05^h34^m31.97^s$  and at a declination (DEC) of  $+22^d00^m52.1^s$ , in the constellation of Taurus (J2000 epoch). The Nebula has a diameter of 6 ly, and is expanding at a rate of about 1,500 kilometers per second. It is also a nearby pulsar wind Nebula (PWN) and the Crab is powered by a 33 ms pulsar that injects relativistic electrons into the Nebula. Synchrotron radiation by the relativistic charged particles ( $e^\pm$ ) results in the emission of radiation from radio to GeV  $\gamma$ -rays, while higher energy (GeV to TeV) gamma rays are thought to result from the Synchrotron Self-Compton (SSC) process, ie inverse-Compton interaction of the high energy  $e^\pm$  with the synchrotron photons emitted by themselves [Gaensler and Slane 2006, de Jager and Harding 1992, de Jager et al 1996, Atoyan and Aharonian 1996, Hillas et al 1998].

The Crab Nebula is considered as the standard candle in VHE  $\gamma$ -ray astronomy due to its strong and steady emission. In the past few years, discovery of variable  $\gamma$ -ray emission from the Crab Nebula has been reported by the AGILE [Tavani et al 2011] and *Fermi*-LAT [Abdo et al 2011] telescopes during September 2010. During this period Crab Nebula flux in 100 MeV to 1 GeV energy band increased by an order of magnitude in less than a day. However, in the TeV energy band, MAGIC and VERITAS telescopes did not see any enhancement in the flux during this period [Mariotti 2010, Ong 2010]. The ARGO-YBJ collaboration have reported enhanced  $\gamma$ -ray signals with a median energy of 1 TeV from the direction of the Crab Nebula, which is consistent with the flares detected by AGILE and *Fermi*-LAT but the increase in flux is below  $5\sigma$  level [Aielli et al 2010, Bartoli et al 2012, Vernetto and for the ARGO-YBJ collaboration 2013]. Another episode of enhanced emission in MeV-GeV energy band, lasting for almost two weeks, took place in March 2013. During this period, *Fermi*-LAT detected a 20-fold increase in the flux of  $\gamma$ -rays for energies above 100 MeV. Again, VHE observations carried by VERITAS during this period did not show any evidence for increase in  $\gamma$ -ray flux [Aliu et al 2014]. The HAWC [Salesa Greus and HAWC Collaboration 2015] detector also did not find any evidence of variations in the Crab flux during the period June 13, 2013 to July 9, 2014. In some of the earlier experiments, also there were reports of rare detection of  $\gamma$ -rays from the direction of Crab Nebula, presumably due to enhanced flux above the detection threshold

[Bhat et al 1986, Acharya et al 1990, 1992, Gupta et al 1978]. Thus, though occasionally variability in the flux of  $\gamma$ -ray was reported in various energy bands, it appears that Crab Nebula is a steady source in TeV energy band [Toor and Seward 1977, Kirsch et al 2005]. Therefore it can still be used as a “standard candle” source for the calibration of ground based atmospheric Cherenkov telescopes.

HAGAR is an array of non-imaging atmospheric Cherenkov telescopes, began its VHE observation of Crab Nebula and other astrophysical sources in the 2008 observing season. HAGAR has successfully detected flares from blazars like Mkn421 [Shukla et al 2012] and Mkn501 [Shukla et al 2015]. This paper discusses the method used in our search for steady  $\gamma$ -rays using wavefront sampling technique. In the non-imaging technique where  $\gamma$  like events can not be directly distinguished from the cosmic ray background (hadron generated) events. The subtraction of cosmic ray background remain always a challenge for the estimation of absolute  $\gamma$ -ray flux. The second most important point is related with observational method, when the sky brightness of  $\gamma$ -ray source and corresponding background regions are different. In order to address the challenges associated with this technique the other data sets which include observations of fictitious sources (dark region of the sky and bright sky region) with special interest to the Crab Nebula region have been studied and discussed in detail. These data sets were used to test and validate the method used in subtraction of cosmic ray background from  $\gamma$ -ray source region.

## 2 HAGAR

The High Altitude GAMMA Ray (HAGAR) observatory consists of an array of seven atmospheric Cherenkov telescopes located at the center and corners of a hexagon inscribed in a circle of 50 meter radius, which is shown in figure-1. Each telescope consists of seven parabolic glass mirrors of 10 mm thickness and 0.9 m diameter having  $f/d=1$ . These mirrors are front coated and average reflectivity in the visible range is around 80%. Each mirror has a UV-blue sensitive XP2268B (Photonis) Photo-multiplier tube (PMT), mounted at its focal point with  $3^\circ$  field of view (FOV) angular mask. The total reflector area of all seven telescopes is about  $31 \text{ m}^2$ . These telescopes, which are based on Alt-Azimuth mounting, are controlled remotely through GUI/Linux based system using 17-bit rotary encoders, stepper motors, Microcontroller-based Motion Control Interface Units (MCIU) etc. The control system allows to achieve a steady state pointing accuracy of 10 arcsec with a maximum slew rate of  $30^\circ$  per minute for each axis and continuous monitoring of the telescope positions. Guide telescopes fitted paraxial to telescope mirrors are used to arrive at a pointing model for each telescope. The co-planarity of all 7 mirrors of a given telescope with its axis is achieved by a series of bright star scans. The over-all accuracy in pointing of the mirrors is about 12 arc minutes. Details of the telescope control and the pointing model of HAGAR array have been extensively discussed [Gothe et al 2013]. The high voltages to PMTs are controlled and

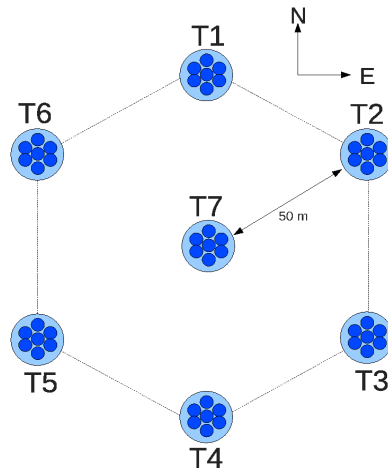


**Fig. 1** Schematic diagram of HAGAR telescope array

monitored through CAEN universal multi-channel power supply system. The analog PMT signals are transmitted to the control room located at the center of the array (below Tel #7) through coaxial cables. The pulses of seven PMTs of a telescope are linearly added to generate a telescope pulse. A CAMAC and VME based data acquisition (DAQ) system has been used for processing of signals from individual PMTs as well as telescope pulses. A DAQ consisting of eight channel Flash ADC (fast waveform digitizer, Acqiris make) system has been used to digitize 7-telescope pulses. A trigger for the initiation of data recording is formed when any four out of seven telescope pulses cross the pre-defined discriminator threshold within a coincidence window of 60 ns. In this paper we restrict our analysis to the data recorded by the digitizer.

### 3 Observations and Data sample

We observed Crab Nebula extensively with HAGAR telescopes since its inception. The observations time period extended from October 2008 to December 2017. The key information, the direction cosine of the shower axis, is derived from the relative time of arrival of Cherenkov shower front at telescopes, which is recorded through 8 bits Agilent (time resolution = 1ns) waveform digitizer. Observations are carried in ON-OFF mode (source followed by its background or vice-versa). The source and corresponding background region are observed for typical duration of 60 minutes each. The declination angle of the cosmic ray background region and the duration of observation are kept same as those of source to have same zenith angle range. In order to assess the performance and systematic in the analysis method several other regions like fixed angle (telescopes parked at some zenith angle) and dark region (fictitious source) of the sky were also observed. Log of observation duration after selection of ON-OFF run pairs taken on the same night and having same zenith angle coverage

**Table 1** Observation Log for Crab Nebula and related runs

Source	Number of ON/OFF run pairs	Duration (hours)
Crab Nebula	241	219.0
Dark region	108	97.5
Fixed angle	98	46.1
Bright sky region	26	24.8

are given in Table - 1. All types of observations (both source and background) were taken on the same night to minimize the effect of sky conditions on PMT counting rates. The night sky condition and count rates of individual PMTs were monitored throughout the observations.

## 4 Analysis

The analysis of the HAGAR data has been performed using in-house developed codes in the IDL programming language. In this technique, analysis of the data is based on the comparison of cosmic-ray events from a  $\gamma$ -ray source region with similar cosmic-ray background region. The complete analysis method is grouped into three sub-sections. These are data reduction, estimation of event arrival direction and extraction of  $\gamma$ -ray signal.

### 4.1 Data reduction

The Acqiris DC271 high speed 8 bit waveform digitizer is configured for 1 nanosecond sampling period, records waveform of PMT pulses at the rate of 1 GHz. The vertical scale of digitizer was configured for 2 Volts with an offset set at positive 875 millivolts. The pre-trigger delay was set for 700 ns and the time stamp for the triggered event is recorded up to microsecond using cPCI GPS clock. A dynamic window approach was used to locate the Cherenkov pulse region in the readout trace of 1000 ns sampling time. A typical waveform produced by the flash ADC as shown in the figure-2 indicates pulse and off-pulse regions. The Cherenkov pulse window is set for 200 ns and remaining traces of waveform is used for the estimation of average night sky background (NSB) during ON-source and OFF-source observation. The figure-3 shows Cherenkov pulse fitted with Log-Normal function. The pulse parameters such as amplitude, rise time, fall time, pulse width (FWHM), pulse charge and pulse arrival time are calculated from the fitted pulse shape. The pulse arrival time is defined as the time at which the pulse amplitude reaches 95% of its absolute maximum.

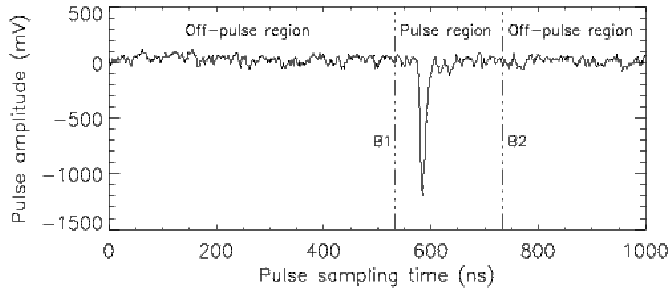


**Fig. 2** Typical Cherenkov (telescope) pulse pattern produced by the flash ADC. The pulses of seven PMTs of a telescope are linearly added to generate a telescope pulse. The B1 (50ns) and B2 (150ns) indicate pre and post time stamps of Cherenkov pulse region with respect to pulse arrival time.

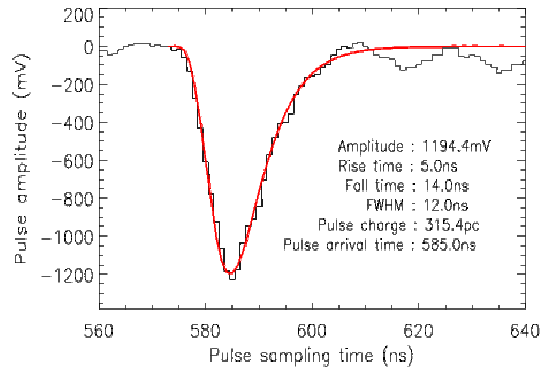


**Fig. 3** Cherenkov pulse fitted with Log-Normal function

#### 4.2 Reconstruction of event arrival direction

The relative arrival times of telescope pulses are used to reconstruct the arrival direction of Cherenkov shower. These relative arrival times are first corrected for a fixed time offset called  $t_{zero}$  ( $T_0$ ). A finite but constant time delay ( $t_{zero}$ ) between telescope channels arises due to the difference in the signal path length, propagation delay in processing electronics and transit time of PMTs. The  $t_{zero}$  values are calculated using data from runs conducted by pointing all the telescopes in a fixed direction, such as Zenith,  $10^\circ$  North,  $10^\circ$  South etc. For each pair of telescopes, we get an equation of the form [Majumdar et al 2003]

$$\chi^2 = \sum w_{ij} (T_0_i - T_0_j - C_{ij})^2 \quad (1)$$

where  $T_0_i$  and  $T_0_j$  are the  $t_{zeros}$  (time offsets),  $C_{ij}$  is mean delay respectively between a pair of  $i^{th}$  and  $j^{th}$  telescope and the  $w_{ij}$  is weight factor. The weight factor  $w_{ij} = 1/\sigma_{ij}^2$  is calculated from  $C_{ij}$  distribution. The  $t_{zeros}$  values are calculated by solving simultaneous equations formed by minimization of  $\chi^2$

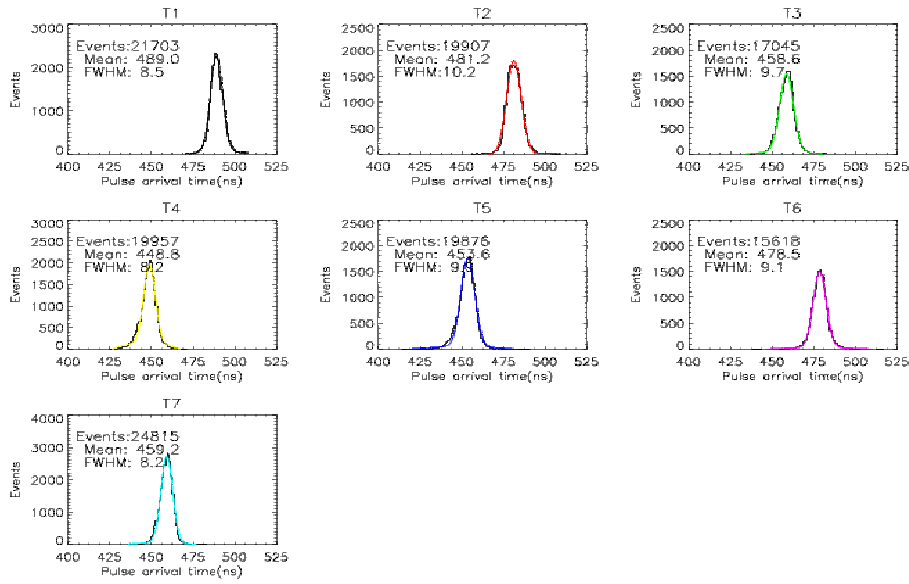


**Fig. 4** Arrival time distribution of telescope T1, T2, T3, T4, T5, T6 and T7 pulses taken from  $10^\circ$  South (Zenith angle= $10^\circ$  and Azimuthal angle= $180^\circ$ ) run # 6053

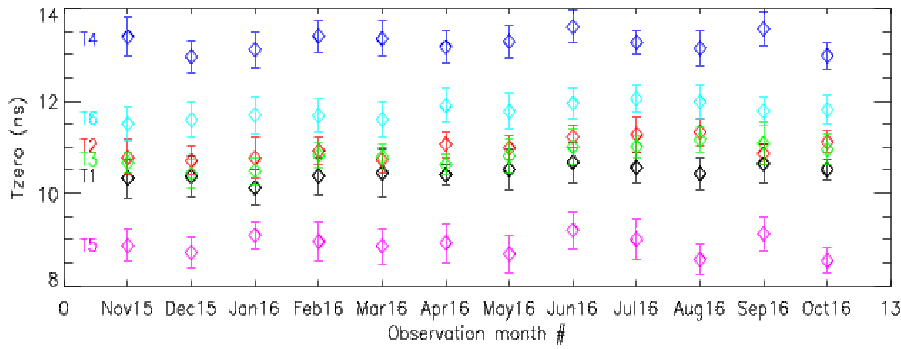


**Fig. 5** Relative time offsets (tzeros) of telescopes T1, T2,...T6 with respect to T7 over period of one year

value. Figure-4 shows the distributions of pulse arrival time taken from the  $10^\circ$  South direction. The variation in the mean arrival time is due to the difference in the geometrical delay arising due to inclination angle, relative difference in the z-height of telescopes and tzeros. The average time delay between two telescope pulses after correction for geometrical delay and z-height from a large sample of data accurately represents the two time-offsets. The data used for estimating the time-offsets of HAGAR telescopes consist of only cosmic ray events. Figure-5 shows the time-offsets of telescopes relative to the telescope T7 over the period of twelve months. The statistical error in the tzeros estimated from different fixed (North, South or Zenith) direction

events is less than a nanosecond. Any other variation in the tzeros of a given telescope could be due to changes in operating (signal path) and climatological conditions. Monthly averaged, time-offsets were used in the estimation of the arrival direction of events collected in different data sets.

In the HAGAR array, arrival direction of the shower is estimated using the plane front approximation [Acharya et al 1993]. The arrival direction of the Cherenkov shower can be estimated by minimization of  $\chi^2$

$$\chi^2 = \sum w_i (lx_i + my_i + nz_i + c(t_i - t_0))^2 \quad (2)$$

where  $x_i, y_i, z_i$  are the coordinates of the  $i^{th}$  telescope,  $l, m, n$  the direction cosines of the shower axis,  $t_i$  the arrival time of the showerfront at this telescope and  $t_0$  is the arrival time of shower front at the origin of the coordinate system. Timing measurement of  $i^{th}$  telescope is weighted ( $w_i = 1/\sigma_i^2$ ), where  $\sigma_i$  is uncertainty in the relative timing measurement of Cherenkov shower wavefront which arises due to shower fluctuation and arrival direction. The values of  $l, m, n$  and  $t_0$  are calculated by solving equations  $\partial\chi^2/\partial l = 0, \partial\chi^2/\partial m = 0, \partial\chi^2/\partial t_0 = 0$  and  $l^2 + m^2 + n^2 = 1$ . The space angle ( $\psi$ ) is an angle between telescope pointing direction and reconstructed direction of the shower and is given by

$$\cos \psi = l_1.l_2 + m_1.m_2 + n_1.n_2 \quad (3)$$

where  $(l_1, m_1, n_1)$  and  $(l_2, m_2, n_2)$  are the direction cosines of telescope pointing and reconstructed direction of the shower. Figure-6 shows the space angle distribution of cosmic ray events for  $10^\circ$  South direction run. Since opening angle or view cone of HAGAR telescope is  $3^\circ$  cosmic ray showers with incidence angle roughly in the range of  $\pm 1.5^\circ$  with respect to the pointing direction can trigger DAQ. The acceptance of showers increases with view cone due to increase in solid angle and detection efficiency of showers decreases with zenith angle due to absorption of showers. The convolution of detection efficiency with incident showers shows maximum around 1 degree. In the figure-6 peak of the space angle distribution occurs at  $0.8 \pm 0.1$  degree and space angles greater than  $3^\circ$  are due to poor fitting of shower wavefront. The space angle distribution of events using CORSIKA [Saha et al 2013] almost overlap in full width at half maximum (FWHM) and peak position with run data. The standard deviation of a Gaussian fit to space angle distribution is obtained and the figure-7 shows the distribution of these standard deviations ( $\sigma$ ) obtained from fixed direction runs. The mean of the distribution is  $0.53 \pm 0.02^\circ$ .

### 4.3 Extraction of $\gamma$ -ray signal

The trigger rate stability is checked as a function of recorded time. Any short term contamination in data which arises due to instrument error or bad sky condition are rejected by clipping run data. The relative arrival times of Cherenkov shower front at telescopes are fitted with a plane and normal to this plane gives the direction of arrival of the shower. If the residue (observed -



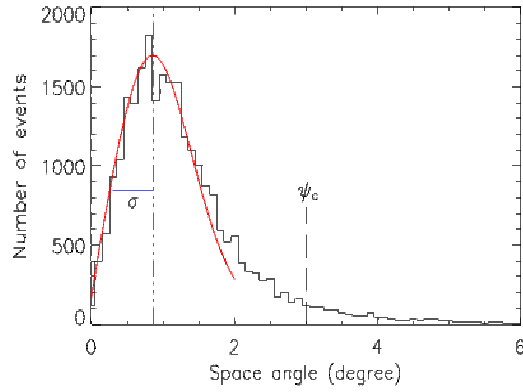


**Fig. 6** Distribution of space angle of events. Data taken from run # 6053 (10 deg South) and observation duration is 60 minutes

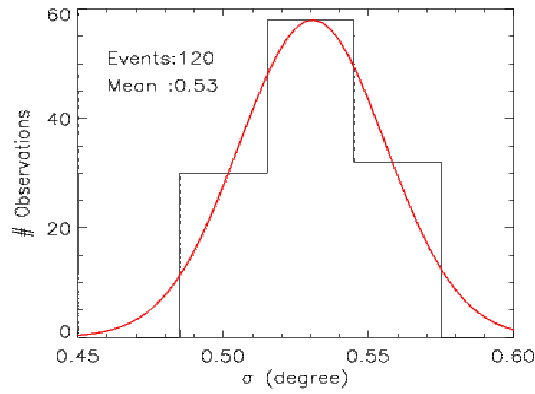


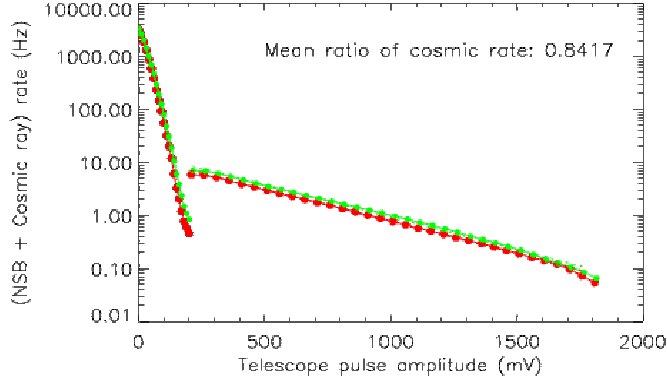
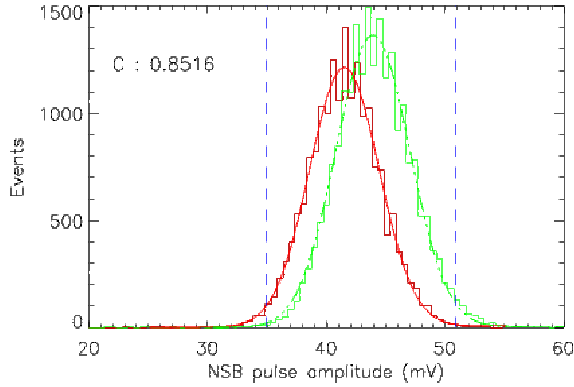
**Fig. 7** Distribution of  $\sigma$  of Gaussian function fit to space angle distributions for  $10^\circ$  North,  $10^\circ$  South and Zenith direction runs

expected) delay is greater than 3 ns for any of the telescopes then same event is reprocessed after rejecting the telescope having largest deviation and this iteration continues till all residues are within the 3 ns or less than four telescopes are available for the angle fit, whichever occurs earlier. In this process almost 10-15% of events get rejected as we need atleast 4 telescopes with valid arrival time of Cherenkov shower front for estimating the arrival direction. The ON-OFF runs are paired based on the overlapping period (hour angle) taken during the same night.

The excess/deficit  $\gamma$ -ray signal is estimated by comparison of events from source direction to its background direction. Data taken with different sky condition or operating condition results in large excess/deficit counts. This difference is neutralized through the normalization of night sky pulses. The Table-2 lists details of two run pairs on fictitious source. The data Set-I corresponds to a run pair taken on the same night, but different region of the sky having the same declination but offset in RA by 75 minutes and data Set-II

**Table 2** Excess/deficit signal from fictitious source runs

Run ID	Set-I		Set-II	
	MJD	5625	5626	6365
RA (HH:MM:SS)	06:50:29	08:05:29	06:50:34	06:50:34
DEC (DD:MM:SS)	20:16:41	20:16:41	22:01:30	22:01:30
Total events	29789	33191	16409	19202
Event rate (Hz)	7.45	8.31	5.36	6.28
Obs. time (minutes)	66.6		51.0	
Rate1 (minute <sup>-1</sup> )	-51.1 ± 3.8		-54.8 ± 3.7	
Constant (C)	0.8984		0.8516	
Rate2 (minute <sup>-1</sup> )	-0.4 ± 3.6		1.1 ± 3.4	

**Fig. 8** Integral event rate of night sky and cosmic Cherenkov light at four-fold trigger condition. The red and green points curve correspond to run ID#6365 and run ID#6371**Fig. 9** Distribution of night sky pulses of a run pair from dark region (data Set-II). The red and green curve correspond to run ID#6365 and run ID#6371

corresponds to a run pair taken on different nights but the same region of the sky. The common observation duration for a run pair is calculated from the overlapped region of zenith angle range. Figure-8 shows a typical integral rate-bias curve in which counting rate (Hz) is plotted as a function of the pulse amplitude. The data points (red and green) correspond to the data Set-II of the Table-2. The steeply falling curve is due to night sky light extracted from the off-pulse region (figure-2) and flat curve is produced from the telescope pulses. The intersection point of the night sky and cosmic ray rate-bias curve represent the bias threshold (200 mV) set for the present analysis. The mean ratio of ON-OFF cosmic-ray rate deviates from unity because the same operating condition could not be maintained during observations.

These runs were taken from the sky region, which is devoid of any known  $\gamma$ -ray source so the excess/deficit count rates from such run pairs must result in a null signal. The run pairs are formed by taking first run as an ON-source (fictitious  $\gamma$ -ray source) and second run as an OFF-source (cosmic ray background) without any prior bias in the selection of the sky region. The rate (Rate1) shows the excess/deficit signal after direct subtraction of OFF-source events from corresponding ON-source events. The excess/deficit signal from such source run pair deviates from the neutrality condition. Therefore OFF-source events must be normalized for the effect which causes a significant difference in the event rate of the regular ON-source and OFF-source runs.

The off-pulse region (figure-2) can be used to compute a suitable normalization factor. Since off-pulse region comprises pulses from the night sky light so effect of change in the operating condition of a run pair can be seen in the distribution of their night sky pulses. Figure-9 shows the amplitude distribution of night sky pulses for run pair of data Set-II. The average amplitude of the night sky pulse was calculated for every event. For this purpose, pulses of an event for given telescope were averaged in the off-pulse region. This average pulse height of a telescope in an event is further averaged over all seven telescopes thus yielding a single average pulse per event. The normalization constant (C) is given by

$$C = \frac{\sum_{l1}^{l2} N_{ON}^{NSB}}{\sum_{l1}^{l2} N_{OFF}^{NSB}} \quad (4)$$

The  $N_{ON}^{NSB}$  and  $N_{OFF}^{NSB}$  are the number of night sky pulses from ON-source and OFF-source directions. Two limits ( $l1, l2$ ) define a common range in which only pulses due to night sky light contribute in the distribution. The normalization constant is estimated for each selected ON-OFF run pair and then the excess/deficit signal is calculated. The sky and operating condition (mostly PMTs high voltages) vary from run to run. The excess/deficit signal from an ON-OFF run pair is given by

$$Signal = \sum_0^{\psi_c} N_{ON} - C * \sum_0^{\psi_c} N_{OFF} \quad (5)$$

The  $\psi_c$  is the upper limit on the space angle. The  $N_{ON}$  and  $N_{OFF}$  are a number of events ( $\psi \leq \psi_c$ ) from the source and background direction and constant C

**Table 3** Excess/deficit signal:Fictitious source observations

	Dark region	Fixed angle
Runs (N)	108	98
Average Event rate (Hz)	7.99±1.31	9.49±2.17
Excess/deficit rate (minute <sup>-1</sup> )	0.01±0.37	-0.02±0.62
$\sigma$	3.43	3.84
Error on mean ( $\frac{\sigma}{\sqrt{N}}$ )	0.33	0.39

is a normalization factor. The excess/deficit rate (Rate2) shows signal after the normalization of OFF-source events.

## 5 Results

### 5.1 Fictitious source

The possibility of systematic effects in the excess/deficit signal due to improper normalization of the night-sky background levels between the ON and OFF source regions of the sky is a major problem for ON-OFF observation technique. The PMT count rate and the trigger rates of each ON-OFF pair are very sensitive to the night sky conditions. The possibility of any systematic error due to the improper normalization of run pair was checked with fictitious source observations. Two types of data sets were used to calculate systematic errors in the detected signal. The fictitious source observations were taken from the different regions of the sky with different brightness. Data sets ‘‘Dark region’’ and ‘‘Fixed angle’’ described in Table-1 represent the fictitious sources.

Results of both fictitious source data sets are listed in Table-3. The figure-10 shows the distribution of  $\gamma$ -ray signal from the fictitious sources. The systematic error in the rate of  $\gamma$ -ray event per minute is about 0.33. In both cases the mean signal is close to zero as expected. The run pairs of data set ‘‘Dark region’’ are from the same brightness region of the sky and devoid of any known VHE source, therefore the  $\gamma$ -ray signal derived by selecting any of the run as ON and the other as OFF and vice versa would give the same null result. The run pairs of data set ‘‘Fixed angle’’ are from the transiting sky region. These runs have effect of varying night sky light, therefore the distribution shown in figure-10 is expected to be broader for the ‘‘Fixed angle’’ runs compared to ‘‘Dark region’’ runs. The statistical error ( $\pm 0.37$  minute<sup>-1</sup>) and systematic error ( $\pm 0.33$  minute<sup>-1</sup>) of the ‘‘dark region’’ runs are relevant for the extraction of signal from a true source as these runs are analogous to regular  $\gamma$ -ray source observations.

### 5.2 Bright sky region

The FOV of HAGAR telescope is 3 degree and the presence of any bright star (say magnitude 3 or 4) directly affects the operating conditions and trig-

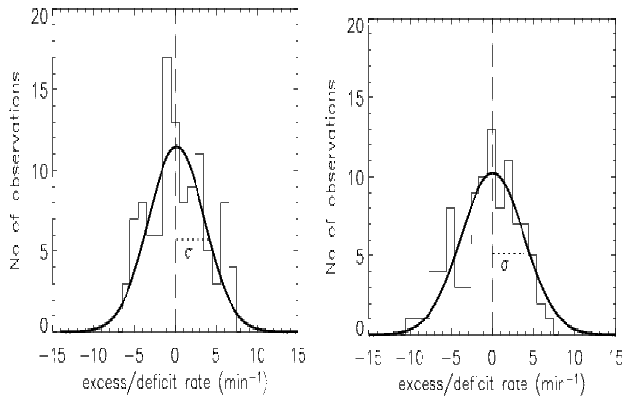


**Fig. 10** Distribution of excess/deficit rates from the run pairs of “Dark region” (left panel) and “Fixed angle” (right panel)

gered events. In a regular observation the high voltages of PMTs are adjusted in such a way that 4-fold chance is less than 1% of trigger rate. When the brightness between ON and OFF regions are comparable or slightly different then PMT voltages are re-adjusted, mostly by a few volts to maintain the chance trigger rate. The sky region with the Crab Nebula +  $\zeta$  Tauri star (apparent magnitude  $V=3.010$ ,  $B-V=-0.164$ ) is brighter than the corresponding background region. In order to maintain a similar count rates of PMTs and low chance rate, the PMTs voltages are re-adjusted, mostly by 50-70 volts between ON and OFF regions. The effects of change in the operating condition between ON-source and OFF-source of Crab runs due to the presence of bright star in the ON-source region were also checked. The data set “Bright sky region” described in Table-1 and sky map<sup>1</sup> shown in figure-11 represent fictitious source ( $RA=05^h35^m36^s$ ,  $DEC=20^d16^m37^s$ ) and background ( $RA=04^h20^m36^s$ ,  $DEC=20^d16^m37^s$ ) regions. Thus, the fictitious source region include  $\zeta$  Tauri star at the same angular offset which is present in regular observations of the Crab Nebula runs and does not include Crab Nebula. These runs with star  $\zeta$  Tauri represent as ON-source and corresponding pair on the background region taken on same night represent as OFF-source. The average event rate from source and background directions are  $6.1 \pm 0.3$  and  $7.3 \pm 0.3$  Hz respectively. Figure-12 shows excess/deficit signal as function of observations. The average excess/deficit count rate from the fictitious source “Bright sky region” is  $0.16 \pm 0.59$  per minute and agree with the null results shown by “Dark region” and “Fixed angle” data sets.

### 5.3 Crab source

The ON-OFF pairs which have common (from zenith/hour angle) duration greater than 30 minutes were used in the final analysis. Figure-13 shows event

<sup>1</sup> <https://freestarcharts.com/messier-1>

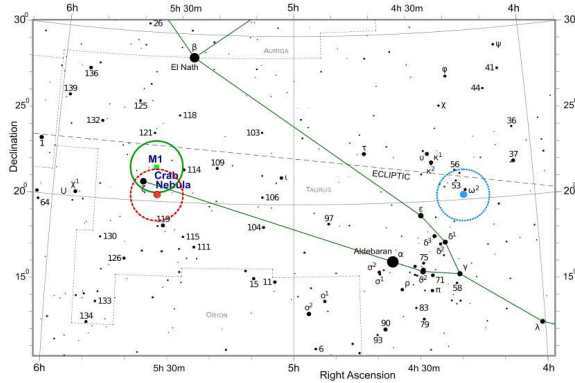


**Fig. 11** Sky map for “Bright sky region” observations. Green circle (continuous line) shows sky region of Crab Nebula observations and red circle (dashed line) and blue circle (dotted line) show sky region of fictitious source observations. The angular offset between Crab Nebula and fictitious source region is 1.75 degree. Size of circle is approximately the FOV of HAGAR telescopes.

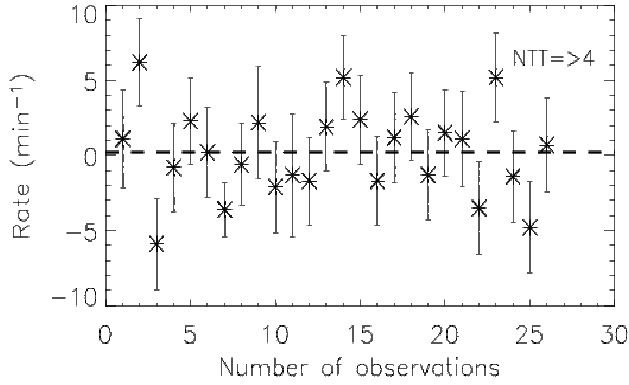


**Fig. 12** Excess/deficit rate per minute from the fictitious source “Bright sky region” direction

rates of ON-OFF runs as a function of the number of observations. Because of slight difference in the operating condition (discussed in §5.2), the event rate of OFF-source run is always higher than ON-source run. The space angle distribution of ON-source events is compared with the corresponding OFF-source events. A cut on the space angle of events is imposed to select events from the source direction. The space angle limit ( $\psi_c$ ) for accepted events is set at  $3^\circ$ , which is the maximum acceptance angle of HAGAR telescope, and hence  $\gamma$ -ray signal is expected to be within this limit for point sources. The normalized background distribution is subtracted from the ON-source distribution and excess/deficit of events is calculated. The analysis results of all selected ON-OFF run pairs is listed in Table-4. The analysis results span over nine years of observation data. The column-5 and column-6 show average event rates of

ON-source and OFF-source runs. The column-7 lists average  $\gamma$ -ray rate detected in each observation year. The statistical significance  $N_\sigma$  was calculated using [Li and Ma 1983], is given by

$$N_\sigma = \frac{N_{ON} - C * N_{OFF}}{\sqrt{N_{ON} + C^2 * N_{OFF}}} \quad (6)$$

where  $N_{ON}$  is number of events from the source direction and  $N_{OFF}$  are number of events from the background direction. The column-8 lists total significance ( $\sigma$ ) detected in each observation period and column-9 lists sensitivity of detecting  $\gamma$ -ray signal. Figure-14 shows estimated  $\gamma$ -ray rate from the Crab Nebula over the period of nine years. Each point in the upper panel of the figure shows estimated  $\gamma$  count rates on daily observation basis and lower panel points show average  $\gamma$  count rates on a time scale of a month. The low operating voltage of PMTs and maximized observation duration during 2015 and 2017 are possible reasons for better stability in the monthly averaged signal. Figure-15 shows the distribution of  $\gamma$ -ray rate per minute from the Crab Nebula. The standard deviation of Gaussian fit is used to estimate the error in the signal detection which is due to long term changes in the weather and instrument maintenance. This standard deviation is 1.87 and the error on mean works out to be 0.13 per minute which is used as systematic error in the present estimation of  $\gamma$ -ray rate. We estimate an average  $\gamma$ -ray rate from the Crab Nebula to be  $4.64 \pm 0.23_{sta} \pm 0.13_{sys}$  per minute at the HAGAR trigger threshold<sup>2</sup> of 230 GeV. Figure-16 shows the significance ( $\sigma$ ) of detected signal as a function of observation time. The total statistical significance has been  $20.3\sigma$  for 219.1 hours of data and results in a detection sensitivity of  $1.24\sigma\sqrt{T}$ , where T is the observation time in hours.

For flux determination, we have calculated the time averaged flux over all the HAGAR observations of the Crab Nebula. Energy threshold and collection area applicable for average zenith angle of  $15^\circ$  was used [Saha et al 2013]. The average flux, thus obtained is  $(1.64 \pm 0.09) \times 10^{-10}$  photons  $\text{cm}^{-2} \text{sec}^{-1}$  for energies above 230 GeV, where the quoted error is only statistical.

The accuracy of the measured  $\gamma$ -ray rate and flux depends on the accuracy of the reconstruction of the arrival direction and normalization of background cosmic ray events in an ON-OFF run pair. Additional uncertainties can arise due to the possible variation of the trigger rates as well as due to offsets in the telescope pointing, large zenith angles of observations and the applied cuts in the event selection process. All these add up to systematic errors.

## 6 Conclusions

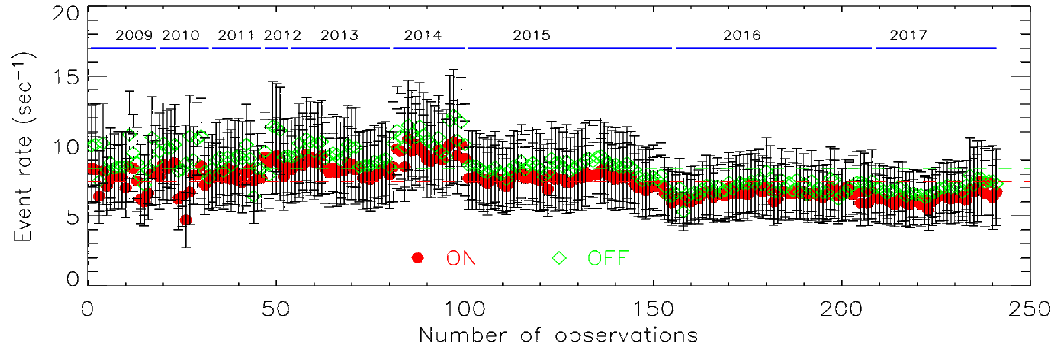
1. The data analysis procedure for the extraction of  $\gamma$ -ray signal using the wavefront sampling HAGAR array has been described in detail. We have tested this data analysis method on dark regions devoid of any known  $\gamma$ -ray

---

<sup>2</sup> Uncertainty in energy threshold is  $\pm 12$  GeV

**Table 4** Excess/deficit signal:Crab Nebula observations

Year	MJD	Runs	Duration (hours)	Average Event rate (Hz)		$\gamma$ -rate $\text{min}^{-1}$	Significance $N_\sigma$	$\frac{\sigma}{\sqrt{T}}$
				ON-source	OFF-source			
2009	55127 - 55188	18	11.2	$7.54 \pm 0.80$	$8.92 \pm 1.04$	$6.13 \pm 0.98$	6.26	1.63
2010	55500 - 55596	14	9.3	$7.55 \pm 1.18$	$9.40 \pm 1.02$	$5.83 \pm 1.14$	5.09	1.63
2011	55861 - 55976	14	9.2	$7.85 \pm 0.39$	$8.75 \pm 0.84$	$4.09 \pm 1.07$	3.85	1.49
2012	56299 - 56332	7	4.6	$8.77 \pm 0.53$	$9.97 \pm 1.32$	$6.08 \pm 1.78$	3.41	1.76
2013	56599 - 56714	27	26.6	$8.41 \pm 0.48$	$9.38 \pm 0.62$	$4.45 \pm 0.71$	6.28	1.52
2014	56956 - 57064	20	19.5	$9.52 \pm 0.57$	$10.66 \pm 0.78$	$5.86 \pm 0.89$	6.55	1.44
2015	57306 - 57456	55	55.7	$7.54 \pm 0.45$	$8.35 \pm 0.61$	$4.64 \pm 0.46$	10.20	1.43
2016	57663 - 57811	53	51.8	$6.55 \pm 0.31$	$7.03 \pm 0.48$	$3.86 \pm 0.43$	8.97	1.19
2017	58043 - 58112	33	31.1	$6.74 \pm 1.15$	$7.21 \pm 1.80$	$4.43 \pm 0.56$	7.91	1.37
Average	All data	241	219.0	$7.47 \pm 1.08$	$8.35 \pm 1.36$	$4.64 \pm 0.23$	20.30	1.24

**Fig. 13** Event rate of Crab ON-OFF runs. The blue horizontal line indicates number of observations in the respective calendar year

sources to show that the method does not show any fake sources or spurious  $\gamma$ -ray signal. It is also verified that the present normalization method can efficiently equalize cosmic ray events in the ON-OFF run pairs.

2. A flux of  $(1.64 \pm 0.09) \times 10^{-10}$  photons  $\text{cm}^{-2} \text{sec}^{-1}$  VHE photons of energies greater than 230 GeV from the Crab Nebula was detected by the HAGAR telescope array at a statistical significance of  $\sim 20\sigma$  over the observation period of 219.1 hours spanning nine years. Figure-17 shows the measured flux which is consistent with earlier detections by Whipple [Hillas et al 1998], MAGIC [Aleksić et al 2015], HESS [Aharonian et al 2006, Holler et al 2015], VERITAS [Kevin Meagher for the VERITAS Collaboration 2015] and ARGO-YBJ [Bartoli et al 2015] telescopes.
3. Referring to figure-14, we do not see any significant evidence for the variation in the detected signals of  $\gamma$ -rays from the Crab Nebula during our observations spanning nine years.
4. Detection of flares from AGNs like Mkn421 [Shukla et al 2012] and Mkn501 [Shukla et al 2015] with the HAGAR telescopes has already established its sensitivity to flaring sources. A long term monitoring of Mkn421 [Sinha et al 2016] with HAGAR has been used in multiwave band studies. The blazar 1ES1959+650 has also been observed during its high active state. The anal-



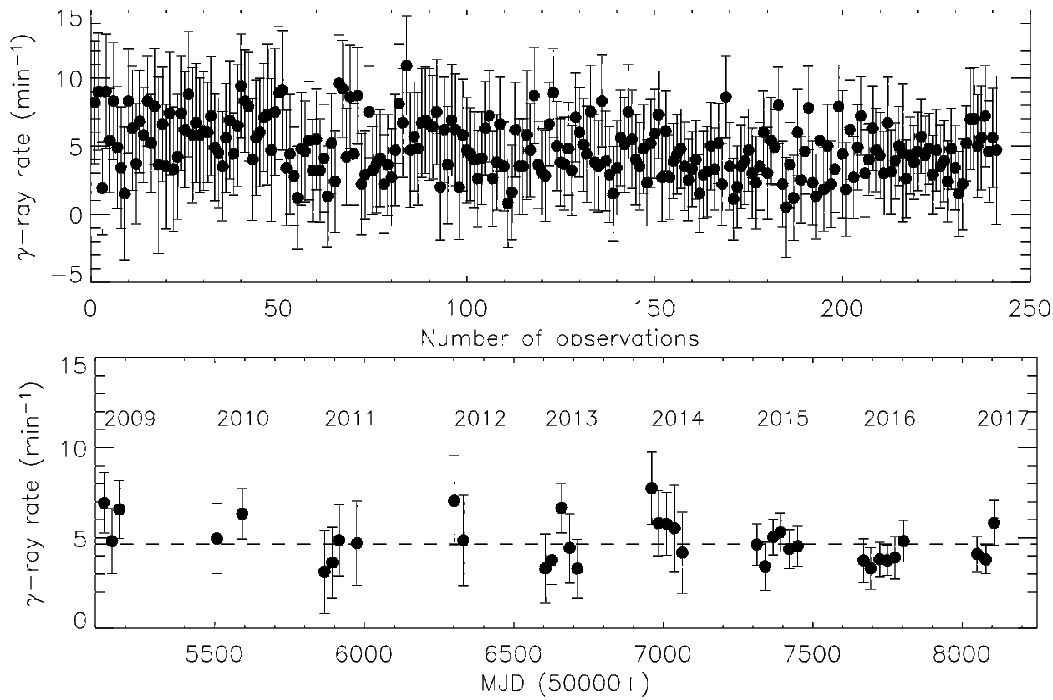


**Fig. 14**  $\gamma$ -ray event rate from the Crab Nebula as function of time. Upper panel: daily light curve, Lower panel: monthly average light curve, The dashed horizontal line is the best fit value to a constant  $\gamma$ -ray rate.

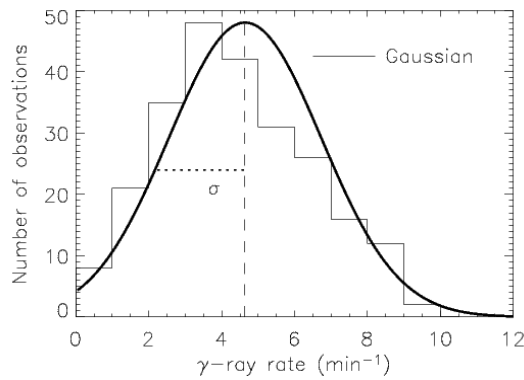


**Fig. 15** Distribution of  $\gamma$ -ray counts.

ysis procedure discussed for signal extraction uses flash ADC data which is much more robust than CAMAC data used in earlier analysis. Improved background subtraction and lower statistical error motivate monitoring of sources below 50% of the Crab flux unit. The HAGAR telescope size and FOV are small but advantage of high altitude location has achieved a lower

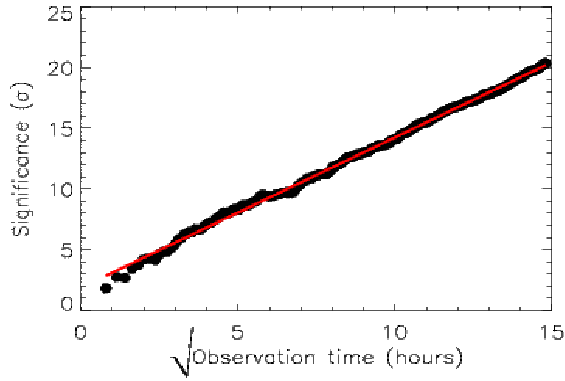


**Fig. 16** Accumulation of  $\gamma$ -ray signal as a function of observation time

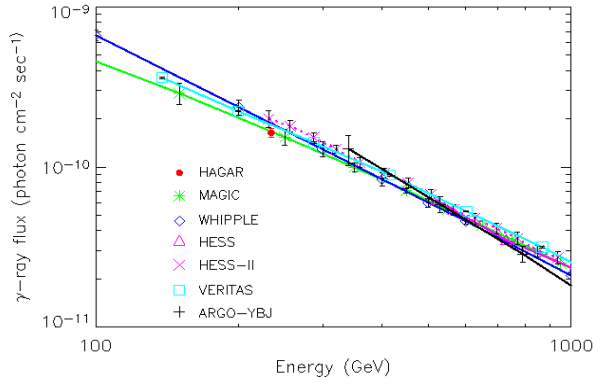


**Fig. 17** Time averaged integral flux detected from the Crab Nebula and compared with measurements from other VHE telescopes

energy threshold. Any alert from a wide field of view (*Fermi*-LAT) or IACT telescopes will be source of interest for HAGAR telescopes. The follow up or dedicated observations based on such alerts would be main targets for future observations.

**Acknowledgements** We thank the engineering and technical staff of IIA and TIFR who have taken part in the construction, installation, maintenance of telescopes and data acquisition setup. Also, we thank the team at the HAGAR site for successful observations and data management. We also thank to Kevin Meagher and Markus Holler for providing VERITAS and HESS-II measurements of the Crab nebula.

## References

- Abdo AA, Ackermann M, Ajello M, Allafort A, Baldini L, Ballet J, Barbiellini G, Bastieri D, Bechtol K, Bellazzini R, Berenji B, Blandford RD, Bloom ED, Bonamente E, Borgland AW, Bouvier A, Brandt TJ, Bregeon J, Brez A, Brigida M, Bruel P, Buehler R, Buson S, Caliandro GA, Cameron RA, Cannon A, Caraveo PA, Casandjian JM, Çelik Ö, Charles E, Chekhtman A, Cheung CC, Chiang J, Ciprini S, Claus R, Cohen-Tanugi J, Costamante L, Cutini S, D'Ammando F, Dermer CD, de Angelis A, de Luca A, de Palma F, Digel SW, do Couto e Silva E, Drell PS, Drlica-Wagner A, Dubois R, Dumora D, Favuzzi C, Fegan SJ, Ferrara EC, Focke WB, Fortin P, Frailis M, Fukazawa Y, Funk S, Fusco P, Gargano F, Gasparrini D, Gehrels N, Germani S, Giglietto N, Giordano F, Giroletti M, Glanzman T, Godfrey G, Grenier IA, Grondin MH, Grove JE, Guiriec S, Hadasch D, Hanabata Y, Harding AK, Hayashi K, Hayashida M, Hays E, Horan D, Itoh R, Jóhannesson G, Johnson AS, Johnson TJ, Khangulyan D, Kamae T, Katagiri H, Kataoka J, Kerr M, Knödlseeder J, Kuss M, Lande J, Latronico L, Lee SH, Lemoine-Goumard M, Longo F, Loparco F, Lubrano P, Madejski GM, Makeev A, Marelli M, Mazziotta MN, McEnery JE, Michelson PF, Mitthumsiri W, Mizuno T, Moiseev AA, Monte C, Monzani ME, Morselli A, Moskalenko IV, Murgia S, Nakamori T, Naumann-Godo M, Nolan PL, Norris JP, Nuss E, Ohsugi T, Okumura A, Omodei N, Ormes JF, Ozaki M, Paneque D, Parent D, Pelassa V, Pepe M, Pesce-Rollins M, Pierbattista M, Piron F, Porter TA, Rainò S, Rando R, Ray PS, Razzano M, Reimer A, Reimer O, Reposeur T, Ritz S, Romani RW, Sadrozinski HFW, Sanchez D, Parkinson PMS, Scargle JD, Schalk TL, Sgrò C, Siskind EJ, Smith PD, Spandre G, Spinelli P, Strickman MS, Suson DJ, Takahashi H, Takahashi T, Tanaka T, Thayer JB, Thompson DJ, Tibaldo L, Torres DF, Tosti G, Tramacere A, Troja E, Uchiyama Y, Vandenbroucke J, Vasileiou V, Vianello G, Vitale V, Wang P, Wood KS, Yang Z, Ziegler M (2011) Gamma-Ray Flares from the Crab Nebula. *Science* 331:739, DOI 10.1126/science.1199705, **1011.3855**
- Acharya BS, Rao MVS, Sivaprasad K, Sreekantan BV, Vishwanath PR (1990) First simultaneous detection of PeV energy burst from the Crab Nebula. *Nature* 347:364, DOI 10.1038/347364a0
- Acharya BS, Bhat PN, Gandhi VN, Ramana Murthy PV, Sathyanarayana GP, Vishwanath PR (1992) Another TeV gamma-ray burst from the Crab pulsar. *A&A* 258:412–414
- Acharya BS, Bhat PN, John AV, Khairatkar SG, Nagesh BK, Rajeev MR, Rao KS, Rao MVS, Reddy A, Sinha S, Sivaprasad K, Stanislaus AJ, Venkateshmurthy BL, Vishwanath PR, Viswanathan K, Unnikrishnan P, Upadhya SS (1993) Angular resolution of the kgf experiment to detect ultra high energy gamma-ray sources. *Journal of Physics G: Nuclear and Particle Physics* 19(7):1053, URL <http://stacks.iop.org/0954-3899/19/i=7/a=016>
- Aharonian F, Akhperjanian AG, Bazer-Bachi AR, Bellicke M, Benbow W, Berge D, Bernlöhr K, Boisson C, Bolz O, Borrel V, Braun I, Breitling F, Brown AM, Bühler R, Büsching I, Carrigan S, Chadwick PM, Chounet

- LM, Cornils R, Costamante L, Degrange B, Dickinson HJ, Djannati-Ataï A, O’C Drury L, Dubus G, Egberts K, Emmanoulopoulos D, Espigat P, Feinstein F, Ferrero E, Fiasson A, Fontaine G, Funk S, Funk S, Gallant YA, Giebels B, Glicenstein JF, Goret P, Hadjichristidis C, Hauser D, Hauser M, Heinzelmann G, Henri G, Hermann G, Hinton JA, Hofmann W, Holleran M, Horns D, Jacholkowska A, de Jager OC, Khélifi B, Komin N, Konopelko A, Kosack K, Latham IJ, Le Gallou R, Lemièrre A, Lemoine-Goumard M, Lohse T, Martin JM, Martineau-Huynh O, Marcowith A, Masterson C, McComb TJJ, de Naurois M, Nedbal D, Nolan SJ, Noutsos A, Orford KJ, Osborne JL, Ouchrif M, Panter M, Pelletier G, Pita S, Pühlhofer G, Punch M, Raubenheimer BC, Raue M, Rayner SM, Reimer A, Reimer O, Ripken J, Rob L, Rolland L, Rowell G, Sahakian V, Saugé L, Schlenker S, Schlickeiser R, Schwanke U, Sol H, Spangler D, Spanier F, Steenkamp R, Stegmann C, Superina G, Tavernet JP, Terrier R, Théoret CG, Tluczykont M, van Eldik C, Vasileiadis G, Venter C, Vincent P, Völk HJ, Wagner SJ, Ward M (2006) Observations of the Crab nebula with HESS. *A&A* 457:899–915, DOI 10.1051/0004-6361:20065351, [astro-ph/0607333](https://arxiv.org/abs/astro-ph/0607333)
- Aielli G, Camarri P, Iuppa R, Santonico R, Bacci C, Branchini P, Budano A, Bussino S, Celio P, de Vincenzi M, James I, Mari SM, Montini P, Pistilli P, Bartoli B, Catalanotti S, D’Ettorre Piazzoli B, di Girolamo T, Iacovacci M, Saggese L, Bernardini P, Bleve C, de Mitri I, Mancarella G, Marsella G, Martello D, Panareo M, Perrone L, Bi XJ, Cao Z, Chen SZ, Chen Y, Feng Z, Gou QB, Guo YQ, He HH, Hu H, Li XX, Liu C, Lu H, Ma XH, Shen PR, Sheng XD, Shi F, Tan YH, Wang B, Wang H, Wu CY, Wu HR, Yao ZG, Zha M, Zhang HM, Zhang J, Zhang J, Zhang Y, Zhu QQ, Calabrese Melcarne AK, Zizzi G, Cappa A, Vallania P, Vernetto S, Cardarelli R, di Sciascio G, Liberti B, Cattaneo C, Salvini P, Creti P, Surdo A, Cui SW, Dai BZ, Liu CQ, Liu J, Yang QY, Yang XC, Zhang L, Zhang P, D’Ali’Staiti G, Chen TL, Danzengluobu, Ding XH, Hu H, Labaciren, Li HJ, Liu MY, Ning CC, Yuan AF, Zhaxisangzhu, Zhaxiciren, Dattoli M, Vigorito C, Feng CF, Li JY, Qu XB, Xue L, Zhang XY, Feng Z, Huang Q, Jia HY, Xu B, Zhou XX, Zhu FR, Galeazzi F, Gargana R, Ruggieri F, Stanescu C, Galeotti P, Giroletti E, Liguori G, Mastroianni S, Rossi E, Pagliaro A (2010) Enhanced TeV gamma ray flux from the Crab Nebula observed. *The Astronomer’s Telegram* 2921
- Aleksić J, Ansoldi S, Antonelli LA, Antoranz P, Babic A, Bangale P, Barrio JA, Becerra González J, Bednarek W, Bernardini E, Biasuzzi B, Biland A, Blanch O, Bonnefoy S, Bonnoli G, Borracci F, Bretz T, Carmona E, Carosi A, Colin P, Colombo E, Contreras JL, Cortina J, Covino S, Da Vela P, Dazzi F, De Angelis A, De Caneva G, De Lotto B, de Oña Wilhelmi E, Delgado Mendez C, Doert M, Dominis Prester D, Dorner D, Doro M, Eiske S, Eisenacher D, Elsaesser D, Fonseca MV, Font L, Frantzen K, Fruck C, Galindo D, García López RJ, Garczarczyk M, Garrido Terrats D, Gaug M, Godinović N, González Muñoz A, Gozzini SR, Hadasch D, Hanabata Y, Hayashida M, Herrera J, Hildebrand D, Hose J, Hrupec D, Idec W, Kadenius V, Kellermann H, Kodani K, Konno Y, Krause J, Kubo H, Kushida J,

- La Barbera A, Lelas D, Lewandowska N, Lindfors E, Lombardi S, López M, López-Coto R, López-Oramas A, Lorenz E, Lozano I, Makariev M, Mallot K, Maneva G, Mankuzhiyil N, Mannheim K, Maraschi L, Marcote B, Mariotti M, Martínez M, Mazin D, Menzel U, Miranda JM, Mirzoyan R, Moralejo A, Munar-Adrover P, Nakajima D, Niedzwiecki A, Nilsson K, Nishijima K, Noda K, Nowak N, Orito R, Overkemping A, Paiano S, Palatiello M, Paneque D, Paoletti R, Paredes JM, Paredes-Fortuny X, Persic M, Prada Moroni PG, Prandini E, Prezioso S, Puljak I, Reinthal R, Rhode W, Ribó M, Rico J, Rodriguez Garcia J, Rügamer S, Saggion A, Saito T, Saito K, Satalecka K, Scalzotto V, Scapin V, Schultz C, Schweizer T, Shore SN, Silanpää A, Sitarek J, Snidaric I, Sobczynska D, Spanier F, Stamatescu V, Stamerra A, Steinbring T, Storz J, Strzys M, Takalo L, Takami H, Tavecchio F, Temnikov P, Terzić T, Tescaro D, Teshima M, Thaele J, Tibolla O, Torres DF, Toyama T, Treves A, Uellenbeck M, Vogler P, Wagner RM, Zanin R, Horns D, Martín J, Meyer M (2015) Measurement of the Crab Nebula spectrum over three decades in energy with the MAGIC telescopes. *Journal of High Energy Astrophysics* 5:30–38, DOI 10.1016/j.jheap.2015.01.002, [1406.6892](#)
- Aliu E, Archambault S, Aune T, Benbow W, Berger K, Bird R, Bouvier A, Buckley JH, Bugaev V, Byrum K, Cerruti M, Chen X, Ciupik L, Connolly MP, Cui W, Dumm J, Errando M, Falcone A, Federici S, Feng Q, Finley JP, Fortin P, Fortson L, Furniss A, Galante N, Gillanders GH, Griffin S, Griffiths ST, Grube J, Gyuk G, Hanna D, Holder J, Hughes G, Humensky TB, Kaaret P, Kertzman M, Khassen Y, Kieda D, Krennrich F, Kumar S, Lang MJ, Lyutikov M, Maier G, McArthur S, McCann A, Meagher K, Millis J, Moriarty P, Mukherjee R, O’Faoláin de Bhróithe A, Ong RA, Otte AN, Park N, Perkins JS, Pohl M, Popkow A, Quinn J, Ragan K, Rajotte J, Reyes LC, Reynolds PT, Richards GT, Roache E, Sembroski GH, Sheidaei F, Smith AW, Staszak D, Telezhinsky I, Theiling M, Tucci JV, Tyler J, Varlotta A, Wakely SP, Weekes TC, Weinstein A, Welsing R, Williams DA, Zajczyk A, Zitzer B (2014) A Search for Enhanced Very High Energy Gamma-Ray Emission from the 2013 March Crab Nebula Flare. *ApJ Letter* 781:L11, DOI 10.1088/2041-8205/781/1/L11, [1309.5949](#)
- Atoyan AM, Aharonian FA (1996) On the mechanisms of gamma radiation in the Crab Nebula. *MNRAS* 278:525–541, DOI 10.1093/mnras/278.2.525
- Bartoli B, Bernardini P, Bi XJ, Bolognino I, Branchini P, Budano A, Melcarne AKC, Camarri P, Cao Z, Cardarelli R, Catalanotti S, Cattaneo C, Chen SZ, Chen TL, Chen Y, Creti P, Cui SW, Dai BZ, Staiti GD, D’Amone A, Danzengluobu, De Mitri I, D’Ettorre Piazzoli B, Di Girolamo T, Ding XH, Di Sciascio G, Feng CF, Feng Z, Feng Z, Galeazzi F, Giroletti E, Gou QB, Guo YQ, He HH, Hu H, Hu H, Huang Q, Iacovacci M, Iuppa R, James I, Jia HY, Labaciren, Li HJ, Li JY, Li XX, Liguori G, Liu C, Liu CQ, Liu J, Liu MY, Lu H, Ma LL, Ma XH, Mancarella G, Mari SM, Marsella G, Martello D, Mastroianni S, Montini P, Ning CC, Pagliaro A, Panareo M, Panico B, Perrone L, Pistilli P, Ruggieri F, Salvini P, Santonico R, Sbrano SN, Shen PR, Sheng XD, Shi F, Surdo A, Tan YH, Vallania P, Vernetto S, Vigorito

- C, Wang B, Wang H, Wu CY, Wu HR, Xu B, Xue L, Yang QY, Yang XC, Yao ZG, Yuan AF, Zha M, Zhang HM, Zhang J, Zhang J, Zhang L, Zhang P, Zhang XY, Zhang Y, Zhao J, Zhaxiciren, Zhaxisangzhu, Zhou XX, Zhu FR, Zhu QQ, Zizzi G (2012) Enhanced TeV gamma ray flux from the Crab Nebula observed by the ARGO-YBJ experiment. *The Astronomer's Telegram* 4258
- Bartoli B, Bernardini P, Bi XJ, Branchini P, Budano A, Camarri P, Cao Z, Cardarelli R, Catalanotti S, Chen SZ, Chen TL, Creti P, Cui SW, Dai BZ, D'Amone A, Danzengluobu, De Mitri I, D'Ettorre Piazzoli B, Di Girolamo T, Di Sciascio G, Feng CF, Feng Z, Feng Z, Gou QB, Guo YQ, He HH, Hu H, Hu H, Iacovacci M, Iuppa R, Jia HY, Labaciren, Li HJ, Liguori G, Liu C, Liu J, Liu MY, Lu H, Ma LL, Ma XH, Mancarella G, Mari SM, Marsella G, Martello D, Mastroianni S, Montini P, Ning CC, Panareo M, Perrone L, Pistilli P, Ruggieri F, Salvini P, Santonico R, Shen PR, Sheng XD, Shi F, Surdo A, Tan YH, Vallania P, Vernetto S, Vigorito C, Wang H, Wu CY, Wu HR, Xue L, Yang QY, Yang XC, Yao ZG, Yuan AF, Zha M, Zhang HM, Zhang L, Zhang XY, Zhang Y, Zhao J, Zhaxiciren, Zhaxisangzhu, Zhou XX, Zhu FR, Zhu QQ, Zizzi G, ARGO-YBJ Collaboration, Striani E (2015) Crab Nebula: Five-year Observation with ARGO-YBJ. *APJ* 798:119, DOI 10.1088/0004-637X/798/2/119, [1502.05665](#)
- Bhat PN, Ramanamurthy PV, Sreekantan BV, Vishwanath PR (1986) A very high energy gamma-ray burst from the Crab pulsar. *Nature* 319:127, DOI 10.1038/319127a0
- de Jager OC, Harding AK (1992) The expected high-energy to ultra-high-energy gamma-ray spectrum of the Crab Nebula. *ApJ* 396:161–172, DOI 10.1086/171706
- de Jager OC, Harding AK, Michelson PF, Nel HI, Nolan PL, Sreekumar P, Thompson DJ (1996) Gamma-Ray Observations of the Crab Nebula: A Study of the Synchro-Compton Spectrum. *ApJ* 457:253, DOI 10.1086/176726
- Gaensler BM, Slane PO (2006) The Evolution and Structure of Pulsar Wind Nebulae. *ARAA* 44:17–47, DOI 10.1146/annurev.astro.44.051905.092528, [astro-ph/0601081](#)
- Gothe KS, Prabhu TP, Vishwanath PR, Acharya BS, Srinivasan R, Chitnis VR, Kamath PU, Srinivasulu G, Saleem F, Kemkar PMM, Mahesh PK, Gabriel F, Manoharan J, Dorji N, Dorjai T, Angchuk D, D'souza AI, Duhan SK, Nagesh BK, Rao SK, Sharma SK, Singh BB, Sudersanan PV, Thsering MT, Upadhyaya SS, Anupama GC, Britto RJ, Cowsik R, Saha L, Shukla A (2013) Pointing of HAGAR telescope mirrors. *Experimental Astronomy* 35:489–506, DOI 10.1007/s10686-012-9319-9
- Gupta SK, Ramana Murthy PV, Sreekantan BV, Tonwar SC (1978) High-energy pulsed gamma rays from pulsars. *ApJ* 221:268–273, DOI 10.1086/156025
- Hillas AM, Akerlof CW, Biller SD, Buckley JH, Carter-Lewis DA, Catanese M, Cawley MF, Fegan DJ, Finley JP, Gaidos JA, Krennrich F, Lamb RC, Lang MJ, Mohanty G, Punch M, Reynolds PT, Rodgers AJ, Rose HJ, Rovero AC,

- Schubnell MS, Sembroski GH, Vacanti G, Weekes TC, West M, Zweerink J (1998) The Spectrum of Teravolt Gamma Rays from the Crab Nebula. *ApJ* 503:744–759, DOI 10.1086/306005
- Holler M, Berge D, van Eldik C, Lenain JP, Marandon V, Murach T, de Naurois M, Parsons RD, Prokoph H, Zaborov D, for the H E S S collaboration (2015) Observations of the Crab Nebula with H.E.S.S. Phase II. arXiv e-prints [1509.02902](#)
- Kevin Meagher for the VERITAS Collaboration (2015) Six years of VERITAS observations of the Crab Nebula. arXiv e-prints [1508.06442](#)
- Kirsch MG, Briel UG, Burrows D, Campana S, Cusumano G, Ebisawa K, Freyberg MJ, Guainazzi M, Haberl F, Jahoda K, Kaastra J, Kretschmar P, Larsson S, Lubiński P, Mori K, Plucinsky P, Pollock AM, Rothschild R, Sembay S, Wilms J, Yamamoto M (2005) Crab: the standard x-ray candle with all (modern) x-ray satellites. In: Siegmund OHW (ed) *UV, X-Ray, and Gamma-Ray Space Instrumentation for Astronomy XIV*, *procspie*, vol 5898, pp 22–33, DOI 10.1117/12.616893, [astro-ph/0508235](#)
- Li TP, Ma YQ (1983) Analysis methods for results in gamma-ray astronomy. *ApJ* 272:317–324, DOI 10.1086/161295
- Majumdar P, Acharya BS, Bhat PN, Chitnis VR, Rahman MA, Singh BB, Vishwanath PR (2003) Angular resolution of the Pachmarhi array of Čerenkov telescopes. *Astroparticle Physics* 18:333–349, DOI 10.1016/S0927-6505(02)00148-2, [astro-ph/0204112](#)
- Mariotti M (2010) No significant enhancement in the VHE gamma-ray flux of the Crab Nebula measured by MAGIC in September 2010. *The Astronomer’s Telegram* 2967
- Ong RA (2010) Search for an Enhanced TeV Gamma-Ray Flux from the Crab Nebula with VERITAS. *The Astronomer’s Telegram* 2968
- Saha L, Chitnis VR, Vishwanath PR, Kale S, Shukla A, Acharya BS, Anupama GC, Bhattacharjee P, Britto RJ, Prabhu TP, Singh BB (2013) A study of the performance parameters of the High Altitude Gamma Ray (HAGAR) telescope system at Ladakh in India. *Astroparticle Physics* 42:33–40, DOI 10.1016/j.astropartphys.2012.11.012
- Salesa Greus F, HAWC Collaboration (2015) Observations of the Crab Nebula with Early HAWC Data. In: 34th International Cosmic Ray Conference (ICRC2015), International Cosmic Ray Conference, vol 34, p 744
- Shukla A, Chitnis VR, Vishwanath PR, Acharya BS, Anupama GC, Bhattacharjee P, Britto RJ, Prabhu TP, Saha L, Singh BB (2012) Multiwavelength study of the TeV blazar Mrk 421 during a giant flare. *A&A* 541:A140, DOI 10.1051/0004-6361/201118569, [1203.3850](#)
- Shukla A, Chitnis VR, Singh BB, Acharya BS, Anupama GC, Bhattacharjee P, Britto RJ, Mannheim K, Prabhu TP, Saha L, Vishwanath PR (2015) Multi-frequency, Multi-epoch Study of Mrk 501: Hints for a Two-component Nature of the Emission. *APJ* 798:2, DOI 10.1088/0004-637X/798/1/2, [1503.02706](#)
- Sinha A, Shukla A, Saha L, Acharya BS, Anupama GC, Bhattacharjee P, Britto RJ, Chitnis VR, Prabhu TP, Singh BB, Vishwanath PR (2016) Long-

- term study of Mkn 421 with the HAGAR Array of Telescopes. *A&A* 591:A83, DOI 10.1051/0004-6361/201628152, [1603.06690](#)
- Tavani M, Bulgarelli A, Vittorini V, Pellizzoni A, Striani E, Caraveo P, Weiskopf MC, Tennant A, Pucella G, Trois A, Costa E, Evangelista Y, Pittori C, Verrecchia F, Del Monte E, Campana R, Pilia M, De Luca A, Donnarumma I, Horns D, Ferrigno C, Heinke CO, Trifoglio M, Gianotti F, Vercellone S, Argan A, Barbiellini G, Cattaneo PW, Chen AW, Contessi T, D'Ammando F, DeParis G, Di Cocco G, Di Persio G, Feroci M, Ferrari A, Galli M, Giuliani A, Giusti M, Labanti C, Lapshov I, Lazzarotto F, Lipari P, Longo F, Fuschino F, Marisaldi M, Mereghetti S, Morelli E, Moretti E, Morselli A, Pacciani L, Perotti F, Piano G, Picozza P, Prest M, Rapisarda M, Rappoldi A, Rubini A, Sabatini S, Soffitta P, Vallazza E, Zambra A, Zanello D, Lucarelli F, Santolamazza P, Giommi P, Salotti L, Bignami GF (2011) Discovery of Powerful Gamma-Ray Flares from the Crab Nebula. *Science* 331:736, DOI 10.1126/science.1200083, [1101.2311](#)
- Toor A, Seward FD (1977) Observation of X-rays from the Crab Pulsar. *ApJ* 216:560–564, DOI 10.1086/155497
- Trimble V (1968) Motions and Structure of the Filamentary Envelope of the Crab Nebula. *AJ* 73:535, DOI 10.1086/110658
- Vernetto S, for the ARGO-YBJ collaboration (2013) Study of the Crab Nebula TeV emission variability during five years with ARGO-YBJ. *ArXiv e-prints* [1307.7041](#)
- Weekes TC, Cawley MF, Fegan DJ, Gibbs KG, Hillas AM, Kowk PW, Lamb RC, Lewis DA, Macomb D, Porter NA, Reynolds PT, Vacanti G (1989) Observation of TeV gamma rays from the Crab nebula using the atmospheric Cerenkov imaging technique. *ApJ* 342:379–395, DOI 10.1086/167599